Applied Catalysis B: Environmental 245 (2019) 743–752

Contents lists available at ScienceDirect

Applied Catalysis B: Environmental

journal homepage: www.elsevier.com/locate/apcatb

Promotion effect and mechanism of the addition of Mo on the enhanced low temperature SCR of NO_x by NH_3 over MnO_x/γ-Al_2O_3 catalysts

Gang Yang[a,b], Haitao Zhao[a,b], Xiang Luo[a,b], Kaiqi Shi[a,b], Haibao Zhao[d], Wenkai Wang[b], Quhan Chen[b], Hua Fan[c,**], Tao Wu[a,b,*]

[a] New Materials Institute, The University of Nottingham Ningbo China, Ningbo, 315100, China
[b] Municipal Key Laboratory of Clean Energy Conversion Technologies, The University of Nottingham Ningbo China, Ningbo, 315100, China
[c] School of Resources Environmental & Chemical Engineering, Nanchang University, Nanchang, 330031, China
[d] Zhejiang Feida Environmental Science & Technology CO., LTD, Zhuji, 311899, China

ARTICLE INFO

Keywords:
Low temperature SCR
$MnMo/\gamma$-Al_2O_3
Mo addition
Promotion effects
Mechanism

ABSTRACT

A series of Mn/γ-Al_2O_3 and Mn_xMo_y/γ-Al_2O_3 catalysts were prepared by using Incipient Wetness Impregnation (IWI) method. The catalytic performance tests showed that the $Mn_3Mo_{1.25}/\gamma$-Al_2O_3 demonstrated a higher SCR performance (NO conversion of around 96%) at a broad low temperature range (150–300 °C). The characterization showed that the addition of Mo to the Mn/γ-Al_2O_3 catalysts promoted the dispersion of MnO_x on the surface of γ-Al_2O_3. The adsorption of NO could form two different species, i.e., nitrites and nitrates, on the surface of the catalyst. The presence of nitrites is beneficial to low temperature SCR. It is found that the existence of Mo in the catalyst favours the formation of Mn^{3+}, which plays a critical role in the adsorption of NH_3 and therefore improves NH_3 adsorption capacity of the MnO_x/γ-Al_2O_3 catalysts. The low temperature SCR of the $Mn_3Mo_{1.25}/\gamma$-Al_2O_3 catalyst was found to mainly follow L-H mechanism, but E-R mechanism also plays a role to some extent. Moreover, it is found that the addition of Mo not only mitigates the deactivation of the catalysts, but also broadens the effective temperature range of the SCR catalysts.

1. Introduction

The emission of nitrogen oxides (NO_x) from combustion processes is associated with a series of severe environmental problems, such as acid rain and ozone depletion, has become an issue of great concern for decades [1–3]. To address these problems, the selective catalytic reduction (SCR) of NO_x by NH_3 has been applied to treat flue gas from stationary and mobile sources [4,5]. At coal-fired power stations, V_2O_5-WO_3/TiO_2 is the most commonly used SCR catalyst. However, the high operating temperature window of 300–400 °C is associated with a variety of problems [6,7], such as the possible oxidation of SO_2 and the high energy consumption [8,9]. Therefore, there is a need for the development of low temperature SCR catalysts, which has attracted a wide attention in recent years [10,11].

The manganese-based catalyst is a good alternative to vanadium-based SCR catalysts, which has demonstrated high catalytic activity and selectivity at low temperature [9,12–20]. Mn-based oxides catalysts, such as MnO_x-CeO_2/meso-TiO_2 [21], MnO_2-(Co_3O_4)/TiO_2 [22] and nano-flaky MnO_x supported on carbon nanotubes [16], have outstanding SCR activity at low temperatures. The addition of transition and/or rare earth metals, such as Fe, Ce and Sb etc, has been found to have positive effects on the performance of these Mn-based catalysts [20,23–26]. However, their operating temperature window was narrow. The development of novel SCR catalysts,which are highly efficient at different temperature levels for different applications, is highly desirable but remains very challenging [14].

Previous studies have shown that the addition of Mo can promote the distribution of active constituents on the support and subsequently enhances the activity of the catalyst [27]. Moreover, most researchers believed that low temperature SCR follows Eley-Rideal (E–R) mechanism [28,29]. However, to date, very little work has been carried out on the addition of molybdenum to manganese-based catalysts (Mn_xMo_y/γ-Al_2O_3) to improve its low temperature SCR performance [30].

In this study, Mo was doped on the Mn/γ-Al_2O_3 catalysts via Incipient Wetness Impregnation (IWI) method aiming at improving their low temperature SCR performance. Systematic characterisation and performance testing were carried out to show the effects of Mo

* Corresponding author at: New Materials Institute, The University of Nottingham Ningbo China, Ningbo, 315100, China.
** Corresponding author.
E-mail addresses: caofanhua@126.com (H. Fan), Tao.wu@nottingham.ac.uk (T. Wu).

https://doi.org/10.1016/j.apcatb.2018.12.080
Received 13 October 2018; Received in revised form 24 December 2018; Accepted 31 December 2018
Available online 02 January 2019
0926-3373/

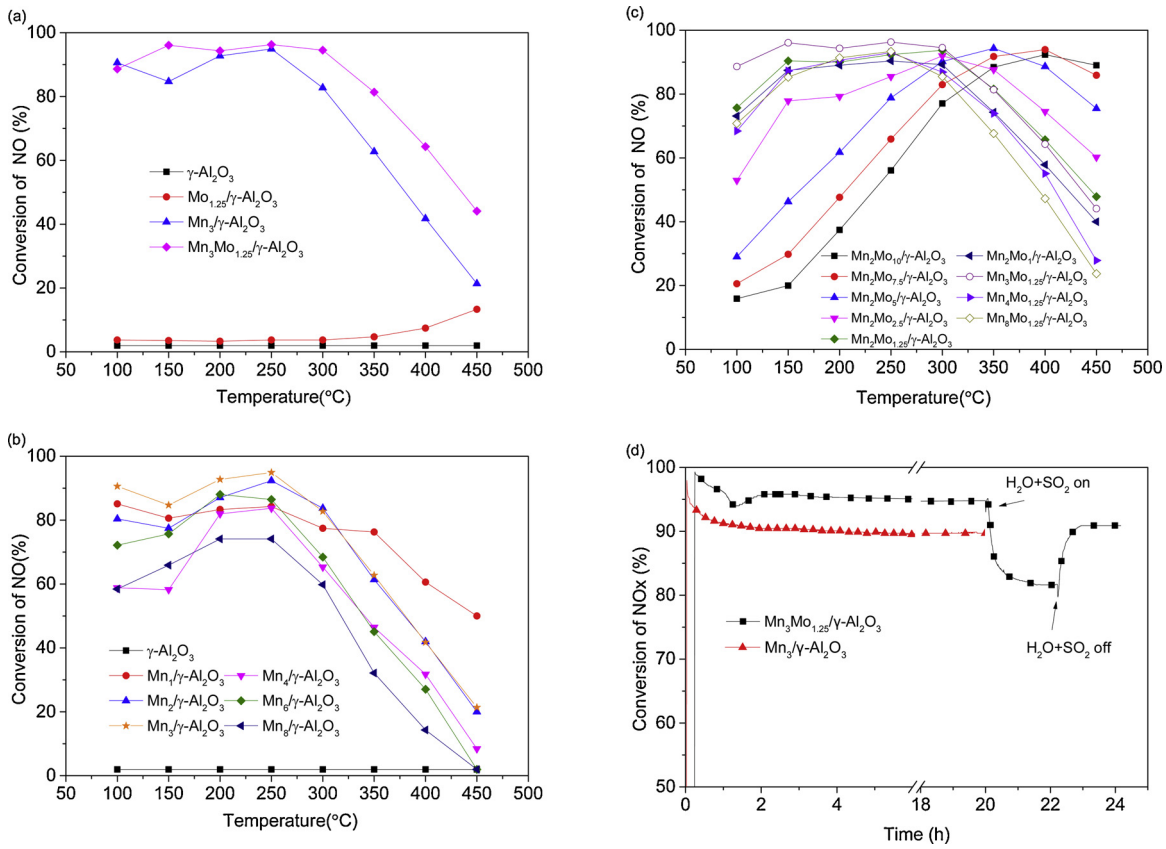

Fig. 1. NO conversion over different catalysts under different gas atmosphere. Reaction condition: (a), (b), (c), (d), $[NH_3] = [NO] = 500$ ppm, $O_2 = 3\%$, N_2 balance, GHSV = 35 000h^{-1}. (d), $SO_2 = 100$ ppm, $H_2O = 5\%$, Temperature 150 °C.

addition on catalytic performance of the $Mn_xMo_y/\gamma\text{-}Al_2O_3$. Moreover, the mechanism of the SCR process at low temperature over the Mo-modified catalyst was investigated.

2. Experimental

2.1. Preparation of catalysts

In this research, a series of Mn-based catalysts with different Mo and Mn loadings supported on $\gamma\text{-}Al_2O_3$ were prepared via IWI method (binary metal catalysts were prepared with a two-step IWI method).

Chemicals of AR grade, such as $Mn(NO_3)_2{\cdot}4H_2O$ and $(NH_4)_6Mo_7O_{24}{\cdot}4H_2O$, were acquired from Sinopharm Chemical Reagent Co., Ltd and used as precursors for the preparation of the catalysts. To prepare a $Mn_xMo_y/\gamma\text{-}Al_2O_3$ catalyst, a controlled amount of $(NH_4)_6Mo_7O_{24}{\cdot}4H_2O$ was loaded on $\gamma\text{-}Al_2O_3$ via IWI method, followed by drying at 120 °C for 24 h and calcination at 520 °C for 12 h. The sample prepared was then impregnated again with certain quantity of the Mn precursor, followed by drying at 120 °C for 24 h and calcination at 520 °C for 12 h. The detailed procedure for the preparation of these catalysts was described elsewhere in our previous research [31,32].

In this study, the $Mn_x/\gamma\text{-}Al_2O_3$ catalysts means x wt% of Mn in the catalyst, while the $Mn_xMo_y/\gamma\text{-}Al_2O_3$ suggests y wt% of Mo in the catalyst.

2.2. Characterization of catalysts

The specific area of samples prepared in this study was characterised by N_2 adsorption/desorption at −196 °C using a Micromeritics ASAP 2020, the procedure of which is described elsewhere in literature [31]. The crystal phases of the catalysts were analysed by using an X-Ray Diffraction (XRD, Bruker D8 Advance) with Cu Kα radiation. Oxidation states of metal species in the catalysts were also analysed using an X-Ray Photoelectron Spectroscopy (XPS Axis Ultra DLD Multifunctional) [33]. The C^{1s} peak at 284.8 eV was used as the standard for calibration. The element compositions of catalysts were analysed by X-Ray Fluorescence (XRF, Bruker s8 TIGER). Morphology, nanostructures and elemental distribution of catalysts were examined using Transmission Electron Microscopy (TEM, FEI Tecnai G2F20). The H_2-temperature programmed reduction (H_2-TPR) was performed to investigate the redox of the samples. Ammonia Temperature Programmed Desorption (NH_3-TPD) method was also carried out to show the quantity and strength of acidic sites on the surface of the catalysts, which was carried out in a Micromeritics AutoChem II 2920 with a heating rate of 10 °C /min and NH_3 adsorption for 30 min at a flowrate of 30 mL/min. NH_3 adsorptions on the surface of catalysts were carried out on a Fourier Transform Infrared Spectroscopy (FTIR, Bruker vertex 70). NO-TPD was performed in a specially designed reactor with gas composition measured by a flue gas analyser (Vario Plus, MRU, Germany).

2.3. Measurement of catalytic activity

The prepared sample was loaded into a fixed-bed reactor and exposed to a simulated flue gas containing NO_x (500 ppm), NH_3 (500 ppm), O_2 (3 vol%), and N_2. The gas hourly space velocity (GHSV) adopted in this study was 3 5000·h^{-1}. Prior to each test, NO_x concentration at the inlet ($[NO_x]_{in}$) was measured to confirm the initial concentration and to minimise experimental errors. The concentration of NO_x at the outlet ($[NO_x]_{out}$) was continuously monitored by the Flue Gas Analyser (MRU Vario Plus and Testo 350, Germany). The NO_x removal efficiency is therefore determined by the following equation:

Table 1
The surface properties of the catalysts.

Catalyst	BET surface area(m^2/g)	Pore volume(cm^3/g)	Pore size(Å)
γ-Al_2O_3	242.2	0.48	79. 7
Mn_2/γ-Al_2O_3	190.02	0.47	99.36
Mn_3/γ-Al_2O_3	216.4	0.45	82.7
Mn_4/γ-Al_2O_3	164.90	0.46	112.33
Mn_6/γ-Al_2O_3	172.18	0.40	88.08
Mn_2Mo_1/γ-Al_2O_3	194.45	0.44	90.86
$Mn_2Mo_{1.25}$/γ-Al_2O_3	207.61	0.46	89.08
$Mn_2Mo_{2.5}$/γ-Al_2O_3	209.65	0.45	86.38
Mn_2Mo_5/γ-Al_2O_3	209.91	0.42	81.16
$Mn_2Mo_{7.5}$/γ-Al_2O_3	209.53	0.42	80.42
Mn_2Mo_{10}/γ-Al_2O_3	189.67	0.37	78.93
$Mn_3Mo_{1.25}$/γ-Al_2O_3	225.7	0.46	80.7
$Mn_4Mo_{1.25}$/γ-Al_2O_3	219.70	0.45	88.11
$Mn_6Mo_{1.25}$/γ-Al_2O_3	192.38	0.41	85.81
Mo_1/γ-Al_2O_3	221.93	0.48	86.69
$Mo_{1.25}$/γ-Al_2O_3	221.18	0.52	94.70
$Mo_{2.5}$/γ-Al_2O_3	223.33	0.46	82.94
Mo_5/γ-Al_2O_3	227.67	0.45	78.85
$Mo_{7.5}$/γ-Al_2O_3	220.37	0.41	75.49
Mo_{10}/γ-Al_2O_3	211.06	0.40	75.00

$$NOx\ removal\ efficiency\ (\%) = \frac{[NOx]_{in} - [NOx]_{out}}{[NOx]_{in}} \times 100\,\% \quad (1)$$

3. Results and discussion

3.1. Catalytic performance

Low temperature catalytic activity of the Mn_x/γ-Al_2O_3 and Mn_xMo_y/γ-Al_2O_3 catalysts was tested in a downflow fixed-bed reactor. NO_x removal efficiency of the four catalysts is illustrated in Fig. 1(a). In Fig. 1(b), Mn_3/γ-Al_2O_3 showed outstanding low temperature NH_3-SCR activity, but the optimal operation temperature was at 250 °C. In order to further improve the low temperature NH_3-SCR activity of the Mn_x/γ-Al_2O_3 catalysts, Mo was added to modify the Mn_x/γ-Al_2O_3 catalysts. In Fig. 1(a), γ-Al_2O_3 and Mo_y/γ-Al_2O_3 did not show any SCR activity in a broad temperature range. It is obvious that the NO conversion of Mn_3/γ-Al_2O_3 was below 90% at 150 °C, above 90% when temperature was raised to 200 and 250 °C, but deteriorated when temperature was raised to higher levels. However, the impregnation of Mo significantly improved the low temperature catalytic performance of the $Mn_3Mo_{1.25}$/γ-Al_2O_3 catalyst, which showed a remarkable promoting effect at 150 °C (NO conversion of 96%), and expanded the effective temperature

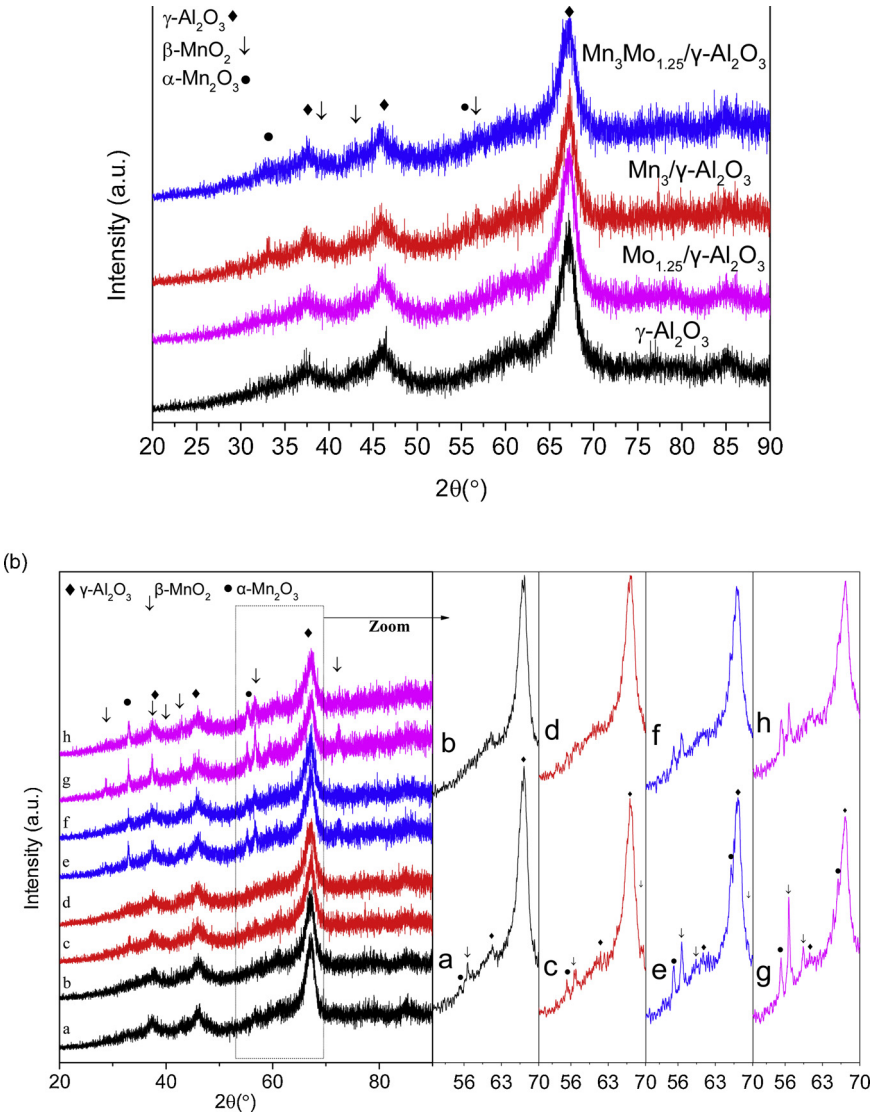

Fig. 2. XRD patterns of catalysts. a. Mn_2/γ-Al_2O_3, b. $Mn_2Mo_{1.25}$/γ-Al_2O_3, c. Mn_3/γ-Al_2O_3, d. $Mn_3Mo_{1.25}$/γ-Al_2O_3, e. Mn_4/γ-Al_2O_3, f. $Mn_4Mo_{1.25}$/γ-Al_2O_3, g. Mn_6/γ-Al_2O_3, h. $Mn_6Mo_{1.25}$/γ-Al_2O_3.

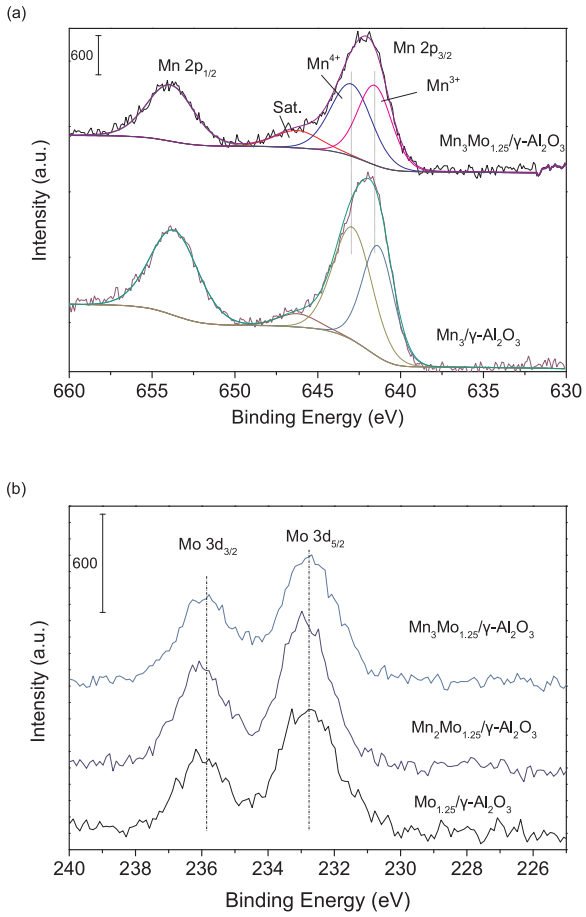

Fig. 3. XPS spectra of MnO_x/γ-Al_2O_3 catalysts before and after Mo addition.

window to 150–300 °C. It was found that at higher Mo loadings, the optimal SCR temperature window started to shift to high temperature levels as shown in Fig. 1(c), which suggests that Mo is a good moderator for the adjustment of effective temperature of the SCR catalysts. Therefore, it can be concluded that the addition of Mo not only promotes the SCR activity of the Mn_x/γ-Al_2O_3 catalyst, but also adjusts the effective temperature range of the catalysts.

The effect of H_2O and SO_2 on the activity of $Mn_3Mo_{1.25}/\gamma$-Al_2O_3 catalysts is shown in Fig. 1(d). When 100 ppm SO_2 and 5% H_2O were introduced into the reactant gas mixture, the NO conversion of the $Mn_3Mo_{1.25}/\gamma$-Al_2O_3 dropped to 81% after 2 h, which is similar to what is reported by other researchers [34–36]. However, when the supply of SO_2 and H_2O was stopped, the NO conversion increased to about 91%. The decrease of NO conversion could be responsible for the deposit of sulphate on the catalyst surface [24]. The results indicate that the $Mn_3Mo_{1.25}/\gamma$-Al_2O_3 is resistant to SO_2 and H_2O. In Fig. 1(d), the durability of $Mn_3Mo_{1.25}/\gamma$-Al_2O_3 and $Mn_3Mo_{1.25}/\gamma$-Al_2O_3 was also conducted at 150 °C. The durability of the $Mn_3Mo_{1.25}/\gamma$-Al_2O_3 was better than that of Mn_3/γ-Al_2O_3. The NO conversion of $Mn_3Mo_{1.25}/\gamma$-Al_2O_3 decreased slightly to 95% after 20 h, which indicated that the addition of Mo enhanced the durability of Mn_x/γ-Al_2O_3 catalysts.

Table 3
The composition (wt.%) of catalysts measured by X-ray fluorescence (XRF).

Catalyst	Mn	Mo	Al	Mn/Al atomic ratio	Mo/Al atomic ratio
$Mn_3Mo_{1.25}/\gamma$-Al_2O_3	3.17	1.33	49.7	0.0313	0.0075
Mn_3/γ-Al_2O_3	3.2	0	50.7	0.0310	0

3.2. Characterization of the catalysts

3.2.1. Effects of Mo addition on Mn dispersion

Structural and morphological properties of the catalysts were investigated by BET and XRD analyses. As shown in Table 1, the specific surface area of the $Mn_3Mo_{1.25}/\gamma$-Al_2O_3 catalyst is larger than that of the Mn_3/γ-Al_2O_3 catalyst, which provides more active sites for low temperature NH_3-SCR reaction. In comparison with pure γ-Al_2O_3, the surface area of the γ-Al_2O_3 loaded with Mo decreased slightly. When the Mo loading was below 5 wt %, the surface area of catalysts increased with the increase in Mo loading, which means that the addition of Mo contributes to the dispersion of active component on the support. However, further increase in Mo loading content prevents this trend. It is clear from Table 1 that when Mo loading is greater than 5 wt %, surface areas of the catalysts decrease with the increase in Mo loading. The low temperature SCR activity dropped with the increase in Mo loading. Therefore, 1.25 wt % of Mo loading is found to be the optimal, which not only enhances the dispersion of Mn on the surface of the catalysts, but also promotes the surface area to certain extent.

XRD spectra of the $Mn_3Mo_{1.25}/\gamma$-Al_2O_3, Mn_3/γ-Al_2O_3, $Mo_{1.25}/\gamma$-Al_2O_3 and γ-Al_2O_3 are shown in Fig. 2 (a). It is clear that the XRD patterns show three different compounds: γ-Al_2O_3 (JCPDS 04-0880), β-MnO_2 (JCPDS 24-0735), α-Mn_2O_3 (JCPDS 24-0508), while the MoO_x does not exist, which is due to its low content. Pijun Gong's et al. [37] claimed that β-MnO_2 has the worst SCR activity among different MnO_2 species, while α-Mn_2O_3 was found to demonstrate high SCR activity and selectivity by many researchers [38,39]. Except for γ-Al_2O_3, the intensity of diffraction peaks of Mn compounds was weak. However, in Fig. 2(b), the diffraction peaks of α-Mn_2O_3, β-MnO_2, especially that of α-Mn_2O_3, started to appear when Mn loading was raised to 3 wt%, and the peaks intensity became higher with the increase in Mn loadings, which means bulk MnO_x species began to form and accumulated on the surface of the catalyst. However, the bulk MnO_x species may occupy a great amount of surface space but show poor low temperature SCR activity [40]. While doping Mo preferentially on the support, the intensity of diffraction peaks intensity of Mn species decreased, as shown in Fig. 2 (a) and (b). It can be concluded that the Mo species could improve the dispersion of MnOx species on the support surface, prevent the formation of large MnO_x bulks, and strengthen the interaction between MnO_x and the support.

3.2.2. XPS, XRF and TEM-EDX

The XPS spectra of Mn 2p (a), Mo 3d (b) are shown in Fig. 3.

Table 2
Binding energy values and surface atomic ratio between Mn 2p for $MnO_x/\ \gamma$-Al_2O_3 catalysts before and after modified by Mo addition.

Catalyst	Binding Energy(eV)		PWHH	Mn^{4+}/Mn^{3+}	Mn/Al atomic ratio (PP)	Mo/Al atomic ratio (PP)
	Mn $2p_{3/2}$					
$Mn_3Mo_{1.25}/\gamma$-Al_2O_3	Mn^{4+}	642.97	2.8	1.08	0.046	0.018
	Mn^{3+}	641.56	2.4			
Mn_3/γ-Al_2O_3	Mn^{4+}	642.84	2.7	1.26	0.062	0
	Mn^{3+}	641.46	2.0			

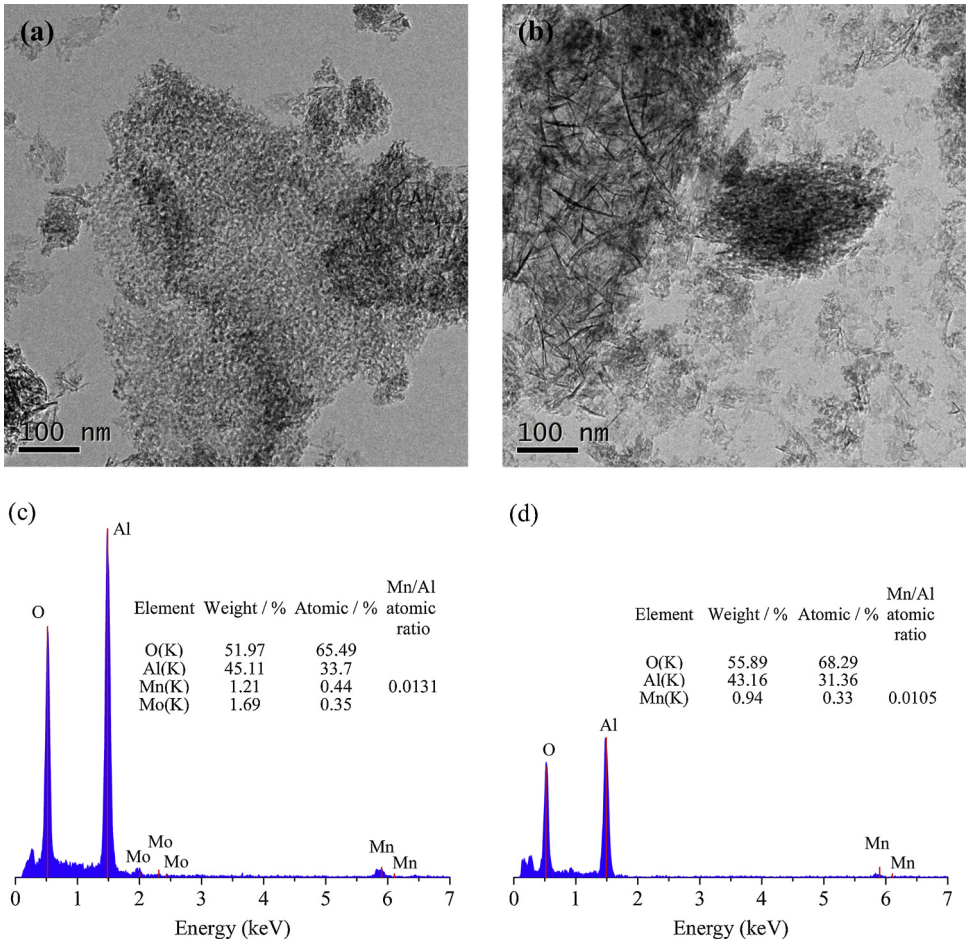

Fig. 4. TEM micrographs(a and b) and EDX (c and d) spectra of $Mn_3/\gamma\text{-}Al_2O_3$ (b and d) and $Mn_3Mo_{1.25}/\gamma\text{-}Al_2O_3$ (a and c).

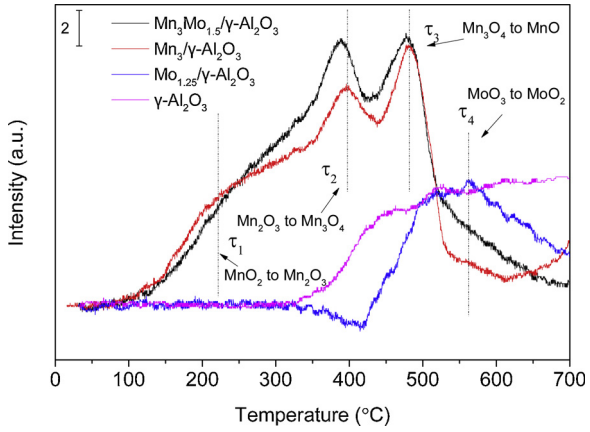

Fig. 5. H_2-TPR profiles over Mo modified $MnO_x/\gamma\text{-}Al_2O_3$ catalysts.

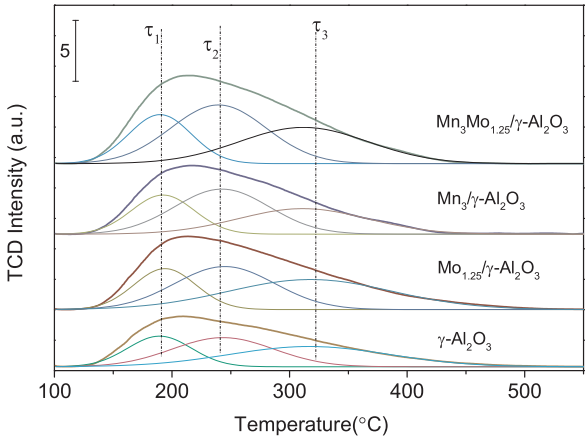

Fig. 6. NH_3-TPD profiles of $Mn_3/\gamma\text{-}Al_2O_3$ catalysts before and after modified by Mo addition.

Different MnO_x species have specific and unique spectra. In Fig. 3(a), $Mn3p_{3/2}$ peaks consist of three MnO_x species, Mn^{4+} (641.5–641.7 eV), Mn^{3+} (541.5–541.7 eV) and satellite [41]. The area ratio, respectively, represent the relative amount of species on the surface. A significant decrease in area ratio of Mn^{4+}/Mn^{3+} from 1.26 to 1.08 was observed as a result of Mo addition, which is consistent with the results of XRD analysis. It can be seen from Table 2 that the $Mn_3Mo_{1.25}/\gamma\text{-}Al_2O_3$ catalyst had a lower Mn/Al atomic ratio. Moreover, XRF and TEM/EDX tests were carried out to show the existence of different species in the catalysts. In Table 3, the mass percentage of Mn, Mo, Al and O is consistent with these species during the preparation of catalysts. Thus, it can be concluded that the Mn was well loaded on the support. In Fig. 4(a) and (b), $Mn_3Mo_{1.25}/\gamma\text{-}Al_2O_3$ is of a more uniform morphology and structure as compared with $Mn_3/\gamma\text{-}Al_2O_3$. No aggradation of MnO_x was formed on the surface of $Mo_3Mo_{1.25}/\gamma\text{-}Al_2O_3$, which means MnOx species have a better dispersion on the surface of $Mo_3Mo_{1.25}/\gamma\text{-}Al_2O_3$. The surface Mn content had a significant increase after the doping of Mo, as shown in Fig. 4(c) and (d). It implies that the addition of Mo strengthens the interactions between MnO_x species and the $\gamma\text{-}Al_2O_3$, promotes the dispersion of MnO_x on the surface of support. In Fig. 3(b), it can be seen that Mo was loaded on the catalysts surface in the form of

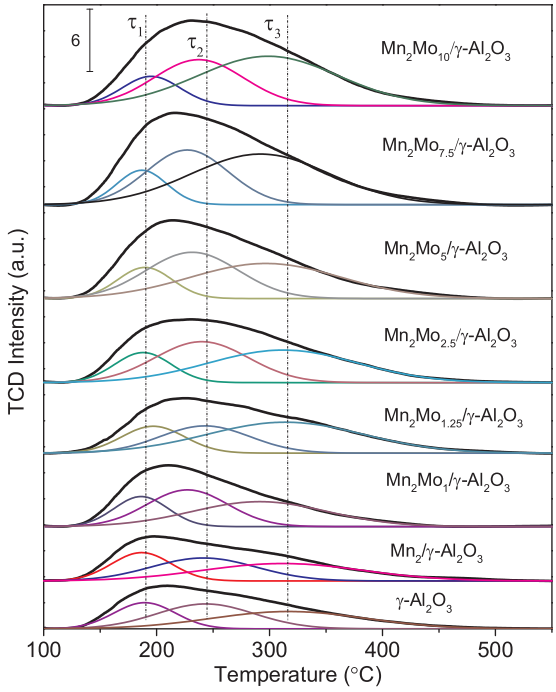

Fig. 7. NH_3-TPD profiles over $Mn_2/\gamma\text{-}Al_2O_3$ catalysts with different Mo loadings.

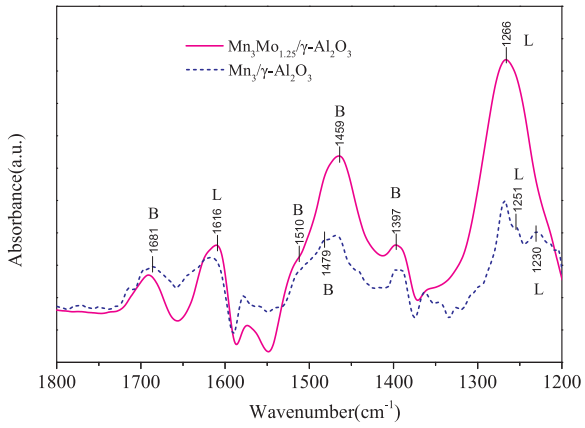

Fig. 8. FTIR spectra of $Mn_3/\gamma\text{-}Al_2O_3$ and $Mn_3Mo_{1.25}/\gamma\text{-}Al_2O_3$ treated in flowing 500 ppm NH_3 at 100 °C until saturation and then purged by N_2.

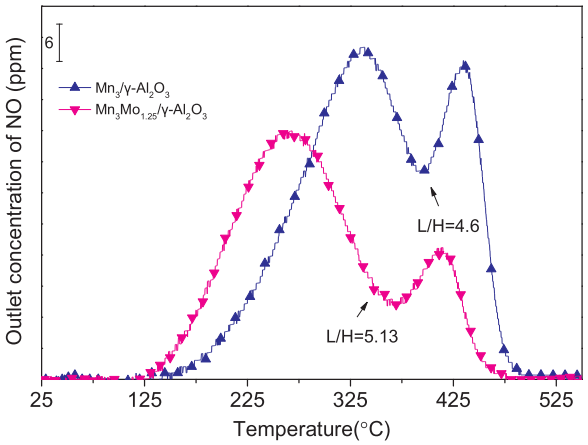

Fig. 9. NO-TPD profiles of the $Mn_3/\gamma\text{-}Al_2O_3$ and $Mn_3Mo_{1.25}/\gamma\text{-}Al_2O_3$.

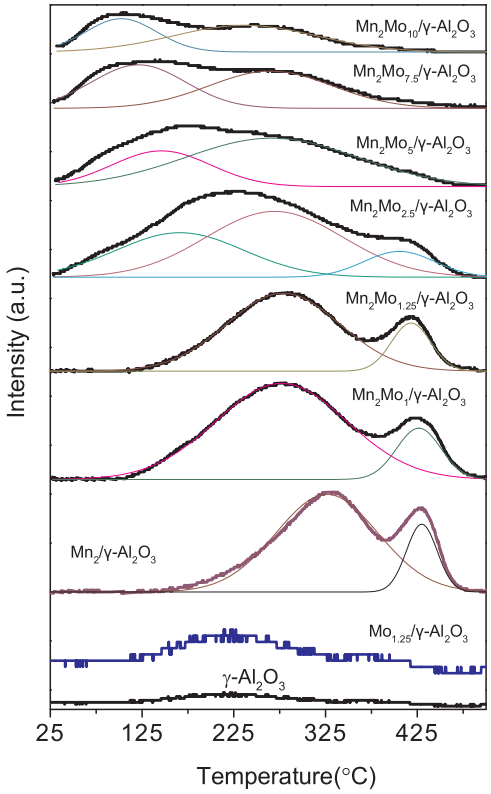

Fig. 10. NO-TPD profiles of the $Mn_2Mo_x/\gamma\text{-}Al_2O_3$.

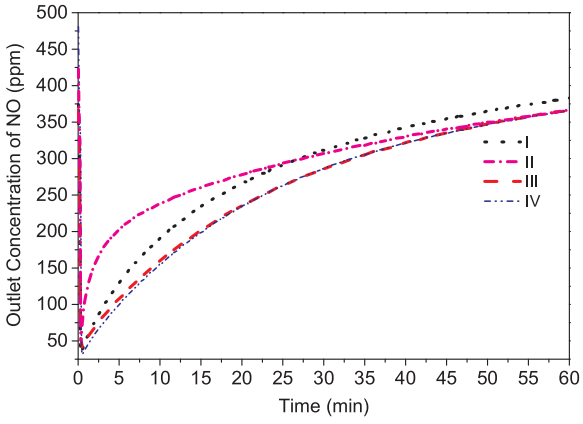

Fig. 11. NO adsorption over the $Mn_3Mo_{1.25}/\gamma\text{-}Al_2O_3$ catalyst.

MoO_3, which is proved by Mo 3d XPS peak at 232.6 eV. In addition, it is speculated that Mo might just act as an accelerant, which is responsible for the formation of active components, its state does not alter on the surface of the support.

3.2.3. H_2-TPR

The H_2-TPR results of the $\gamma\text{-}Al_2O_3$, $Mo_{1.25}/\gamma\text{-}Al_2O_3$, $Mn_3/\gamma\text{-}Al_2O_3$, $Mn_3Mo_{1.25}/\gamma\text{-}Al_2O_3$ are shown in Fig. 5. There are four distinct reduction peaks, τ_1, τ_2, τ_3, τ_4, which are corresponding to the reduction of MnO_2 to Mn_2O_3, Mn_2O_3 to Mn_3O_4, Mn_3O_4 to MnO and MoO_3 to MoO_2 respectively [42]. Additionally, the curve of $\gamma\text{-}Al_2O_3$ did not change significantly except for a noticeable drift at the high temperatures.

Comparing $Mn_3Mo_{1.25}/\gamma\text{-}Al_2O_3$ with $Mn_3/\gamma\text{-}Al_2O_3$, the temperature of τ_2, τ_3 decreases, which suggests that Mn_2O_3 has a stronger interaction with the support in $Mn_3Mo_{1.25}/\gamma\text{-}Al_2O_3$. The intensity of τ_2 and τ_3 also increased. Based on observations, it is speculated that the Mo in catalysts promotes the formation of Mn_2O_3, which is consistent with the

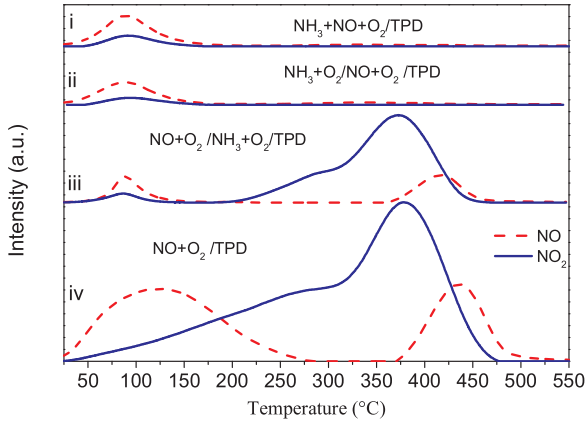

Fig. 12. TPD profiles of the NO adsorption over the $Mn_3Mo_{1.25}/\gamma$-Al_2O_3 catalyst.

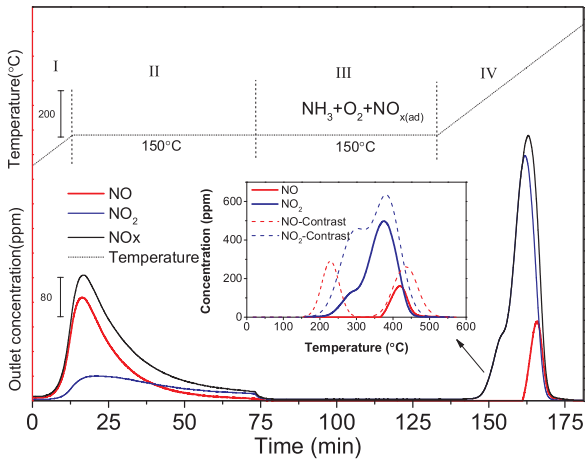

Fig. 13. TPD profiles of NO adsorption over the $Mn_3Mo_{1.25}/\gamma$-Al_2O_3 catalyst, Process I: TPD from 25 to 150 °C; Process II: N_2 purging for 60 min; Process III: adsorbed NO reacted with NH_3; Process IV: TPD from 150 °C to 630 °C.

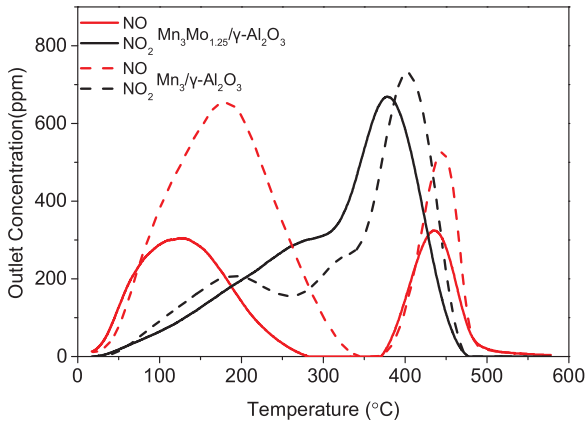

Fig. 14. Effect of O_2 on the NO adsorption over the Mn_3/γ-Al_2O_3 and $Mn_3Mo_{1.25}/\ \gamma$-Al_2O_3 catalyst.

results of XRD and XPS analyses. Normally, only the NH_3 being adsorbed on the Lewis acid site of Mn^{3+} shows low temperature SCR activity and can be activate to -NH_2 [5]. The -NH_2 takes part in the SCR reaction which suggests that the more Mn_2O_3 the catalyst has, the more Mn^{3+} Lewis acid sites are formed, which subsequently promotes low temperature SCR, while the MnO_2 plays a less important role in the low temperature SCR reaction. In contrast, Mn_2O_3 dominated the selective catalytic reduction performance at low temperature, which agreed well with the theory proposed by De Fang [43]. Therefore, it could be concluded that the addition of Mo could promote low temperature SCR activity of the Mn/ γ-Al_2O_3 catalyst by enabling the formation of more Lewis acid sites.

3.2.4. NH_3-TPD and FTIR

The amount and strength of surface acid sites of Mn_3/γ-Al_2O_3 catalysts before and after Mo addition were investigated using NH_3-TPD, which is shown in Fig. 6. There are three distinct peaks, which could be divided into weak, medium and strong acid sites, respectively. The temperature range of τ_1, τ_2 and τ_3 is 150–250 °C, 250–400 °C and 400–500 °C respectively. The $Mn_3Mo_{1.25}/\gamma$-Al_2O_3 had higher intensity at all peaks, which suggests more medium and strong acid sites existed.

Moreover, catalytic activity of the Mn_x/γ-Al_2O_3 catalysts with different Mo loadings was investigated as shown in Fig. 7. The strong and medium acid sites of catalyst increase significantly with the increase in Mo loadings. It is also found that a higher Mo loading led to a higher catalytic temperature of the catalysts in Fig. 1(c). Therefore, the low Mo content (1.25 wt%) favoured the low temperature SCR.

Fig. 8 shows the FTIR spectra of NH_3 adsorption over Mn_3/γ-Al_2O_3 and $Mn_3Mo_{1.25}/\gamma$-Al_2O_3 catalysts at 100 °C. For $Mn_3Mo_{1.25}/\gamma$-Al_2O_3, two stronger bands at 1266 and 1465 cm^{-1} and two relatively weaker bands at 1616 and 1681 cm^{-1} can be observed. The bands at 1230, 1251, 1266, 1616 cm^{-1} can be assigned to bending vibrations of N—H bonds in the NH_3 linked to Lewis acidic sites [44]. The bands at 1397 cm^{-1} are almost the same, resulted from over NH_3 adsorption on γ-Al_2O_3 [45]. The bands at 1459 and 1479 cm^{-1} are observed due to NH_3 adsorbed on Brönsted acidic sites. What's more, an amide(-NH_2) species also is observed at 1510 cm^{-1}. The bands at 1616 cm^{-1} (assigned to Lewis acidic sites) and 1681 cm^{-1} (assigned to Brönsted acidic sites mainly) mainly come from NH_3 adsorption on γ-Al_2O_3. In the previous report [46], molybdenyl species were unsaturated on the catalyst surface and were deranged easily by adsorption of ammonia. In Fig. 8, it can be seen that Lewis and Brönsted acidic sites at 1266 and 1465 cm^{-1} are significantly enhanced after the modification of Mo. This confirms what was found in NH_3-TPD analysis.

3.2.5. NO-TPD

Fig. 9 shows the NO-TPD profiles of the Mn_3/γ-Al_2O_3 catalyst before and after Mo addition. Two desorption peaks can be observed in Fig. 9, which contain a broad peak in the low temperature region (LT-peak) and a strong peak at higher temperature region (HT-peak). The nitroso species forms from the adsorbed NO at LT-peak will react with ammonia [45]. In contrast, the nitro compounds formed from the NO adsorbed at HT-peak only decompose at high temperature and react with –NH_2 [47]. Therefore, the area ratio between LT-peak and HT-peak could be utilized to evaluate the activity of SCR catalyst and investigate the mechanism of catalytic process. In Fig. 9, after the addition of Mo, there is a shift in LT-peak and HT-peak toward lower temperature region and the height of peaks decrease, which indicates that the $Mn_3Mo_{1.25}/\gamma$-Al_2O_3 has a lower SCR activity temperature. In addition, the area ratio between LT-peak and HT-peak increased from 4.6 to 5.13, which means that more nitroso species formed on the $Mn_3Mo_{1.25}/\gamma$-Al_2O_3 so that higher low temperature SCR activity.

Fig. 10 shows that the LT-peak of Mn catalyst shifted to lower temperature region with the Mo loading increased to 2.5 wt% and a new desorption peak formed below 200 °C. With the increase in Mo loading to 10 wt%, the center of the new peak shifted to below 100 °C. Meanwhile, the intensity of HT-peaks weakened gradually and disappeared when the Mo loading was 7.5 wt%. This suggests that the addition of Mo had a significant influence on the adsorption of NO.

3.2.6. Mechanism of low temperature SCR over Mo-modified Mn-based catalysts

Four sets of NO adsorption and desorption experiment were carried out to investigate the adsorption of NH_3 and NO on the $Mn_3Mo_{1.25}/\gamma$-

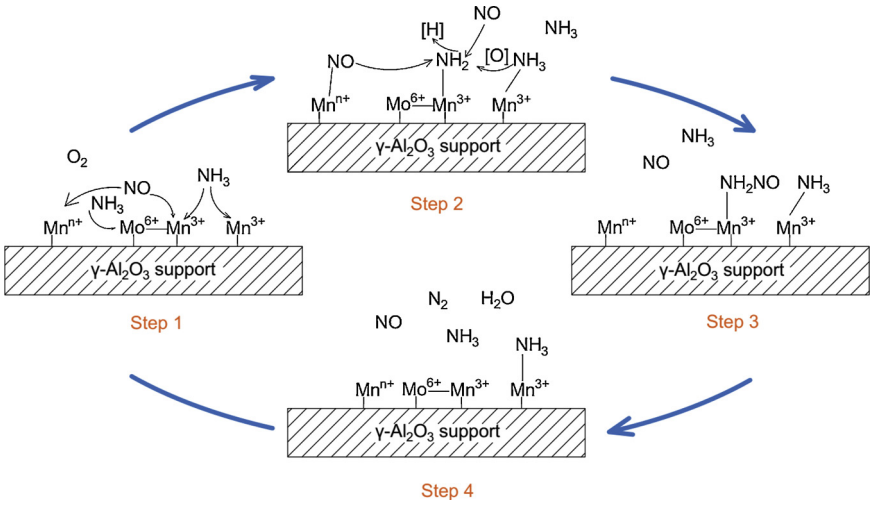

Fig. 15. Low temperature SCR reaction mechanism model.

Al_2O_3 catalysts.

I: The adsorption of NH_3 (500 ppm) +NO (500 ppm) +O_2 (3%) at 25 °C for 1 h, and then purged with N_2 until outlet concentration of NO became below 5 ppm, followed by performing TPD process at 10 °C/min;

II: The adsorption of NH_3 (500 ppm) + O_2 (3%) at 25 °C for 1 h, switched to the adsorption of NO (500 ppm) + O_2 (3%) at 25 °C for 1 h, and then purged with N_2 until outlet concentration of NO became below 5 ppm, followed by performing TPD process at 10 °C /min;

III: The adsorption of NO (500 ppm) +O_2 (3%) at 25 °C for 1 h, switched to the adsorption of NH_3 (500 ppm) + O_2 (3%) at 25 °C for 1 h, and then purged with N_2 until outlet concentration of NO became below 5 ppm, followed by performing TPD Process at 10 °C /min;

IV: The adsorption of NO (500 ppm) +O_2 (3%) at 25 °C for 1 h, and then purged with N_2 until outlet concentration of NO became below 5 ppm, followed by performing TPD Process at 10 °C /min.

In Fig. 11, Curve III coincides with Curve IV resulted from the adsorption of NO on the fresh catalyst. However, Curve I shifted as compared with Curves III and IV when NH_3 and NO were simultaneously introduced, which indicates that NH_3 adsorbs on certain sites competitively with NO. Curve II shifted up significantly in the first 25 min, and then shifted down to the level of curve III and IV. It can therefore be concluded that some of the adsorption sites are occupied randomly by NH_3 owing to NH_3 preferentially adsorbed on the catalyst. According to the calculation, the adsorption capacity of Curve I is larger than that of Curve II, which is attributed to gas phase NH_3 being competitively adsorbed with NO on the catalyst surface. Therefore, the adsorption sites of the catalysts could be classified into four types: Type 1, adsorbs NH_3 preferentially; Type 2, adsorbs NO preferentially; Type 3, adsorbs NH_3 competitively, and Type 4, random adsorption sites, on which both NH_3 and NO can be adsorbed depending on their molecular movement.

As shown in Fig. 12, TPD Curves i and ii do not show high temperature desorption peak of NO and NO_2. TPD Curves iii and iv are similar, but low temperature desorption peaks of curve iii for NO are weak and high temperature desorption peaks also shift. Compared Curve i with iii, TPD results do not show high temperature desorption peaks, which indicates that bidentate nitrate and bridge nitrate are not easy to form on the surface treated by NH_3 [5]. It is speculated that O_2 will accelerate the formation of these stable NO complexes, which only react with NH_3 at high temperature and are responsible for the deactivation of SCR catalysts.

It is generally believed that SCR reaction starts with the adsorption of NH_3. But the mechanisms of low temperature SCR for catalysts with different active components and support are different. Marban et al. [48] suggested that there are two different SCR mechanisms associated with different NH_3 species. In Fig. 12, NO-TPD peaks disappear in Curves i and ii, which is attributed to the reaction between NO and ad-NH_3 on the catalyst surface. As shown in Fig. 13, the $Mn_3Mo_{1.25}/\gamma$-Al_2O_3 catalyst adsorbed NO for 1 h and then carried out TPD test from 25 °C to 150 °C (Process I), followed by purging with N_2 for 1 h (Process II). In Process III, NH_3 and O_2 were introduced, and temperature was kept at 150 °C. In Process IV, TPD test was carried out from 150 °C to 630 °C. In order to compare, a similar test without Process III was taken into consideration, which is also shown in Fig. 13 (dashed line). The amount of NO_x being adsorbed at low temperature around 250 °C decreased, even disappeared, and high temperature species were also reduced to some extent, which directly proves that low temperature SCR proceeds between the adsorbed NH_3 species and the adsorbed NO species via Langmuir-Hinshelwood (L-H) mechanism.

In this study, the addition of Mo was found to improve NH_3 adsorption capacity of the catalyst. With the increase in Mo loadings, the amount of surface acid sites increased, which is vital to SCR reaction. In Fig. 14, when in the presence of gas phase O_2, the adsorption peaks of NO and NO_2 decrease. Therefore, it can be concluded that the addition of Mo could reduce NO adsorption on the catalysts surface but do not result in a lower low temperature SCR activity. Instead, the low temperature SCR efficiency of the $Mn_3Mo_{1.25}/\gamma$-Al_2O_3 is much higher than that of the Mn_3/γ-Al_2O_3 catalyst. Additionally, in Fig.12, Curve II shows a small desorption peak at 100 °C as compared with Curve III. This means that the NOx being desorbed reacted with the NH_3 that is adsorbed on the catalyst when the temperature was raised. Therefore, it is illustrated that low temperature SCR reaction could proceed via Eley-Rideal (E–R) path.

It is clear that the $Mn_3Mo_{1.25}/\gamma$-Al_2O_3 catalyst performed outstanding low temperature SCR activity as a result of Mo addition. It can be concluded that the addition of Mo improves the properties of the catalysts in several aspects. Firstly, the addition of Mo species to the catalyst inhibits the growth of MnO_x bulks, therefore leads to the good dispersion of MnO_x on the γ-Al_2O_3 surface. Secondly, the addition of Mo enhances the formation of Mn_2O_3 on the catalyst, which accelerates the formation of intermediates, whereafter the -NH_3 is transformed into -NH_2 via H-abstraction. Thirdly, the addition of Mo on the catalysts mitigates the deactivation of the catalysts. In Fig. 13, NO adsorbed species at HT-Peak region were very difficult to react with NH_3 at 150 °C. The reason is that these NO formed some complexes (bridged and bidentate nitrates) that are thermally stable. However, the addition of Mo could inhibit the transformation of nitrites into nitrates thus slow down the self-deactivation of the catalysts.

Therefore, the low temperature SCR reaction is composed of 4 steps

as shown in Fig. 15: Step 1, the adsorption of NH_3 and NO on the surface of the catalysts; Step 2, the H-abstraction of adsorbed NH_3, resulting in the formation of -NH_2 species as well as the formation of reactive nitrites from the adsorbed NO species; Step3, the -NH_2 species reacted with nitrites or gas phase NO via L–H and E–R mechanism, forming intermediate products -NH_2NO, and Step4, -NH_2NO decomposed into N_2 and H_2O.

4. Conclusions

In this study, the $Mn_3Mo_{1.25}/\gamma$-Al_2O_3 catalyst achieved a high NO conversion of around 96% at 150–300 °C. It is found that the addition of Mo to Mn-based SCR catalyst could not only inhibit the growth of MnO_x bulks, favour the formation of Mn^{3+} state and promote the NH_3 adsorption capacity of the catalyst, but also act as a moderator to adjust the effective operating temperature window of the SCR reaction, which could be achieved by adjusting Mo loading. Moreover, the addition of Mo was found to mitigate the deactivation of the catalysts. The study on SCR mechanism showed that the low temperature SCR starts from the adsorption of NH_3 on Mn^{3+} sites. The low temperature SCR followed mainly E-R mechanism, but L-H mechanism also plays a role to some extent.

Acknowledgements

National Key R&D Program of China (2017YFB0603202) is acknowledged for partially sponsored this research. Authors 1 and 2 contributed equally to this work.

References

[1] F. Cao, J. Xiang, S. Su, P. Wang, S. Hu, L. Sun, Ag modified Mn–Ce/γ-Al_2O_3 catalyst for selective catalytic reduction of NO with NH_3 at low-temperature, Fuel Process. Technol. 135 (2015) 66–72.
[2] G. Busca, L. Lietti, G. Ramis, F. Berti, Chemical and mechanistic aspects of the selective catalytic reduction of NO_x by ammonia over oxide catalysts: a review, Appl. Catal. B 18 (1998) 1–36.
[3] L. Sun, Q. Cao, B. Hu, J. Li, J. Hao, G. Jing, X. Tang, Synthesis, characterization and catalytic activities of vanadium–cryptomelane manganese oxides in low-temperature NO reduction with NH_3, Appl. Catal. A Gen. 393 (2011) 323–330.
[4] J.A. Dumesic, N.Y. Topsøe, H. Topsøe, Y. Chen, T. Slabiak, Kinetics of selective catalytic reduction of nitric oxide by ammonia over Vanadia/Titania, J. Catal. 163 (1996) 409–417.
[5] W.S. Kijlstra, D.S. Brands, E.K. Poels, A. Bliek, Mechanism of the selective catalytic reduction of NO with NH_3 over MnO_x/Al_2O_3 I. Adsorption and desorption of the single reaction components, J. Catal. 71 (1997) 208–218.
[6] S. Niksa, A. Freeman Sibley, Predicting the multipollutant performance of utility SCR systems, Ind. Eng. Chem. Res. 49 (2010) 6332–6341.
[7] S.S.R. Putluru, L. Schill, A. Godiksen, R. Poreddy, S. Mossin, A.D. Jensen, R. Fehrmann, Promoted V_2O_5/TiO_2 catalysts for selective catalytic reduction of NO with NH_3 at low temperatures, Appl. Catal. B 183 (2016) 282–290.
[8] Q.-l. Chen, R.-t. Guo, Q.-s. Wang, W.-g. Pan, W.-h. Wang, N.-z. Yang, C.-z. Lu, S.-x. Wang, The catalytic performance of $Mn/TiWO_x$ catalyst for selective catalytic reduction of NO_x with NH_3, Fuel 181 (2016) 852–858.
[9] W. Sjoerd Kijlstra, M. Biervliet, E.K. Poels, A. Bliek, Deactivation by SO_2 of MnO_x/Al_2O_3 catalysts used for the selective catalytic reduction of NO with NH_3 at low temperatures, Appl. Catal. B 16 (1998) 327–337.
[10] S.S.R. Putluru, L. Schill, A.D. Jensen, B. Siret, F. Tabaries, R. Fehrmann, Mn/TiO_2 and $Mn–Fe/TiO_2$ catalysts synthesized by deposition precipitation—promising for selective catalytic reduction of NO with NH_3 at low temperatures, Appl. Catal. B 165 (2015) 628–635.
[11] H. Zhao, X. Mu, C. Zheng, S. Liu, Y. Zhu, X. Gao, T. Wu, Structural defects in 2D MoS_2 nanosheets and their roles in the adsorption of airborne elemental mercury, J. Hazard. Mater. 366 (2019) 240–249.
[12] W.S. Kijlstra, D.S. Brands, E.K. Poels, A. Bliek, Mechanism of the selective catalytic reduction of NO by NH_3 over MnO_x/Al_2O_3 I. Adsorption and desorption of the single reaction, J. Catal. 171 (1997) 208–218.
[13] Y.J. Kim, H.J. Kwon, I.-S. Nam, J.W. Choung, J.K. Kil, H.-J. Kim, M.-S. Cha, G.K. Yeo, High deNO_x performance of Mn/TiO_2 catalyst by NH_3, Catal. Today 151 (2010) 244–250.
[14] F. Kapteijn, L. Singoredjo, A. Andreini, J.A. Moulijn, Activity and selectivity of pure manganese oxides in the selective catalytic reduction of nitric oxide with ammonia, Appl. Catal. B 3 (1994) 173–189.
[15] J. Zhu, A. Thomas, Perovskite-type mixed oxides as catalytic material for NO removal, Appl. Catal. B 92 (2009) 225–233.
[16] C. Fang, D. Zhang, S. Cai, L. Zhang, L. Huang, H. Li, P. Maitarad, L. Shi, R. Gao, J. Zhang, Low-temperature selective catalytic reduction of NO with NH_3 over nanoflaky MnOx on carbon nanotubes in situ prepared via a chemical bath deposition route, Nanoscale 5 (2013) 9199–9207.
[17] L. Yan, Y. Liu, K. Zha, H. Li, L. Shi, D. Zhang, Scale–activity relationship of MnOx-FeOy nanocage catalysts derived from prussian blue analogues for low-temperature NO reduction: experimental and DFT studies, ACS Appl. Mater. Interfaces 9 (2017) 2581–2593.
[18] K. Zha, L. Kang, C. Feng, L. Han, H. Li, T. Yan, P. Maitarad, L. Shi, D. Zhang, Improved NOx reduction in the presence of alkali metals by using hollandite Mn–Ti oxide promoted Cu-SAPO-34 catalysts, Environ. Sci. Nano 5 (2018) 1408–1419.
[19] C. Li, X. Tang, H. Yi, L. Wang, X. Cui, C. Chu, J. Li, R. Zhang, Q. Yu, Rational design of template-free MnOx-CeO_2 hollow nanotube as de-NOx catalyst at low temperature, Appl. Surf. Sci. 428 (2018) 924–932.
[20] X. Hu, L. Huang, J. Zhang, H. Li, K. Zha, L. Shi, D. Zhang, Facile and template-free fabrication of mesoporous 3D nanosphere-like $Mn_xCo_{3-x}O_4$ as highly effective catalysts for low temperature SCR of NO_x with NH_3, J. Mater. Chem. A 6 (2018) 2952–2963.
[21] K. Zha, S. Cai, H. Hu, H. Li, T. Yan, L. Shi, D. Zhang, In situ DRIFTs investigation of promotional effects of tungsten on MnOx-CeO_2/meso-TiO_2 catalysts for NOx reduction, J. Phys. Chem. C 121 (2017) 25243–25254.
[22] L. Huang, X. Hu, S. Yuan, H. Li, T. Yan, L. Shi, D. Zhang, Photocatalytic preparation of nanostructured MnO_2-(Co_3O_4)/TiO_2 hybrids: the formation mechanism and catalytic application in SCR deNOx reaction, Appl. Catal. B 203 (2017) 778–788.
[23] R. Jin, Y. Liu, Z. Wu, H. Wang, T. Gu, Low-temperature selective catalytic reduction of NO with NH_3 over Mn-Ce oxides supported on TiO_2 and Al_2O_3: a comparative study, Chemosphere 78 (2010) 1160–1166.
[24] G. Qi, R.T. Yang, Low-temperature selective catalytic reduction of NO with NH_3 over iron and manganese oxides supported on titania, Appl. Catal. B 44 (2003) 217–225.
[25] N.-z. Yang, R.-t. Guo, W.-g. Pan, Q.-l. Chen, Q.-s. Wang, C.-z. Lu, The promotion effect of Sb on the Na resistance of Mn/TiO_2 catalyst for selective catalytic reduction of NO with NH_3, Fuel 169 (2016) 87–92.
[26] L. Liu, C. Zheng, J. Wang, Y. Zhang, X. Gao, K. Cen, NO adsorption and oxidation on Mn doped CeO_2 (111) surfaces: a DFT+ U study, Aerosol Air Qual. Res. 18 (2018) 1080-1088+ ap1081.
[27] H. Zhao, X. Mu, G. Yang, M. George, P. Cao, B. Fanady, S. Rong, X. Gao, T. Wu, Graphene-like MoS_2 containing adsorbents for Hg^0 capture at coal-fired power plants, Appl. Energy (2017).
[28] F. Cao, S. Su, J. Xiang, P. Wang, S. Hu, L. Sun, A. Zhang, The activity and mechanism study of Fe–Mn–Ce/γ-Al_2O_3 catalyst for low temperature selective catalytic reduction of NO with NH_3, Fuel 139 (2015) 232–239.
[29] L. Chen, J. Li, M. Ge, DRIFT study on cerium− Tungsten/Titiania catalyst for selective catalytic reduction of NOx with NH_3, Environ. Sci. Technol. 44 (2010) 9590–9596.
[30] S. Zhang, B. Zhang, B. Liu, S. Sun, A review of Mn-containing oxide catalysts for low temperature selective catalytic reduction of NOx with NH_3: reaction mechanism and catalyst deactivation, RSC Adv. 7 (2017) 26226–26242.
[31] H. Zhao, X. Luo, J. He, C. Peng, T. Wu, Recovery of elemental sulphur via selective catalytic reduction of SO_2 over sulphided CoMo/γ-Al_2O_3 catalysts, Fuel 147 (2015) 67–75.
[32] H. Zhao, G. Yang, X. Gao, C. Pang, S.W. Kingman, T. Wu, Hg^0 capture over CoMoS/γ-Al_2O_3 with MoS_2 nanosheets at low temperatures, Environ. Sci. Technol. (2015).
[33] C. Zhou, X. Liu, C. Wu, Y. Wen, Y. Xue, R. Chen, Z. Zhang, B. Shan, H. Yin, W.G. Wang, NO oxidation catalysis on copper doped hexagonal phase $LaCoO_3$: a combined experimental and theoretical study, J. Chem. Soc. Faraday Trans. 16 (2014) 5106–5112.
[34] Q. Yan, S. Chen, C. Zhang, Q. Wang, B. Louis, Synthesis and catalytic performance of $Cu1Mn_{0.5}Ti_{0.5}O_x$ mixed oxide as low-temperature NH_3-SCR catalyst with enhanced SO_2 resistance, Appl. Catal. B 238 (2018) 236–247.
[35] Z. Liu, J. Zhu, S. Zhang, L. Ma, S.I. Woo, Selective catalytic reduction of NO_x by NH_3 over MoO_3-promoted CeO_2/TiO_2 catalyst, Catal. Commun. 46 (2014) 90–93.
[36] B. Shen, X. Zhang, H. Ma, Y. Yao, T. Liu, A comparative study of Mn/CeO_2, Mn/ZrO_2 and Mn/Ce-ZrO_2 for low temperature selective catalytic reduction of NO with NH3 in the presence of SO_2 and H_2O, J. Environ. Sci. 25 (2013) 791–800.
[37] P. Gong, J. Xie, D. Fang, D. Han, F. He, F. Li, K. Qi, Effects of surface physicochemical properties on NH_3-SCR activity of MnO_2 catalysts with different crystal structures, Chinese J. Catal. 38 (2017) 1925–1934.
[38] J. Xiang, L. Wang, F. Cao, K. Qian, S. Su, S. Hu, Y. Wang, L. Liu, Adsorption properties of NO and NH_3 over MnO_x based catalyst supported on γ-Al_2O_3, Chem. Eng. J. 302 (2016) 570–576.
[39] L. Cheng, Y. Men, J. Wang, H. Wang, W. An, Y. Wang, Z. Duan, J. Liu, Crystal facet-dependent reactivity of α-Mn_2O_3 microcrystalline catalyst for soot combustion, Appl. Catal. B 204 (2017) 374–384.
[40] H.-L. Koh, H.-K. Park, Characterization of MoO_3–V_2O_5/Al_2O_3 catalysts for selective catalytic reduction of NO by NH_3, J. Ind. Eng. Chem. 19 (2013) 73–79.
[41] O.A. Bulavchenko, T.N. Afonasenko, P.G. Tsyrul'nikov, S.V. Tsybulya, Effect of heat treatment conditions on the structure and catalytic properties of MnOx/Al_2O_3 in the reaction of CO oxidation, Appl. Catal. A Gen. 459 (2013) 73–80.
[42] K. Li, R. Wang, J. Chen, Hydrodeoxygenation of anisole over silica-supported Ni_2P, MoP, and NiMoP catalysts, Energy Fuels 25 (2011) 854–863.
[43] D. Fang, J. Xie, H. Hu, H. Yang, F. He, Z. Fu, Identification of MnOx species and Mn valence states in MnOx/TiO_2 catalysts for low temperature SCR, Chem. Eng. J. 271 (2015) 23–30.
[44] L. Ma, Y. Cheng, G. Cavataio, R.W. McCabe, L. Fu, J. Li, In situ DRIFTS and temperature-programmed technology study on NH_3-SCR of NOx over Cu-SSZ-13 and Cu-SAPO-34 catalysts, Appl. Catal. B 156-157 (2014) 428–437.

[45] W.S. Kijlstra, D.S. Brands, H.I. Smit, E.K. Poels, A. Bliek, Mechanism of the selective catalytic reduction of NO with NH_3 over $MnOx/Al_2O_3$ II. Reactivity of adorbed NH_3 and NO complexes, J. Catal. 171 (1997) 219–230.
[46] Z. Liu, S. Zhang, J. Li, L. Ma, Promoting effect of MoO_3 on the NOx reduction by NH_3 over CeO_2/TiO_2 catalyst studied with in situ DRIFTS, Appl. Catal. B 144 (2014) 90–95.
[47] G. Marbán, T. Valdés-Solís, A.B. Fuertes, Mechanism of low-temperature selective catalytic reduction of NO with NH_3 over carbon-supported Mn_3O_4: role of surface NH_3 species: SCR mechanism, J. Catal. 226 (2004) 138–155.
[48] G. Marban, T. Valdes-Solis, A.B. Fuertes, Mechanism of low temperature selective catalytic reduction of NO with NH_3 over carbon-supported Mn_3O_4 Active phase and role of surface NO species, J. Chem. Soc. Faraday Trans. 6 (2004) 453–464.